Biomaterials 32 (2011) 6588–6594

Contents lists available at ScienceDirect

Biomaterials

journal homepage: www.elsevier.com/locate/biomaterials

Nanosheet-based titania microspheres with hollow core-shell structure encapsulating horseradish peroxidase for a mediator-free biosensor

Qing Xie, Yingying Zhao, Xu Chen, Haimei Liu, David G. Evans, Wensheng Yang*

State Key Laboratory of Chemical Resource Engineering, Beijing University of Chemical Technology, Beijing 100029, China

ARTICLE INFO

Article history:
Received 1 May 2011
Accepted 16 May 2011
Available online 12 June 2011

Keywords:
Biosensor
Enzyme immobilization
Nanosheet-based titania
Hollow core-shell structure
Horseradish peroxidase
Direct electron transfer (DET)

ABSTRACT

Nanosheet-based titania (TiO_2) microspheres with a hollow core-shell structure have been synthesized and employed to immobilize horseradish peroxidase (HRP) in order to fabricate a mediator-free biosensor. The morphology and structure of the TiO_2 microspheres were characterized by X-ray diffraction, scanning electron microscopy and transmission electronic microscopy. A possible growth mechanism has been proposed. Spectroscopic and electrochemical measurements revealed that the TiO_2 microspheres are an immobilization support with biocompatibility for enzymes, affording good enzyme stability and bioactivity. Due to the nanosheet-based hollow core-shell structure of the TiO_2 microspheres, the direct electron transfer of HRP is facilitated and the resulting biosensor displayed good performance for the detection of H_2O_2, with both a low detection limit of 0.05 μM and a wide linear range of 0.4–140 μM, as well as a fast response and excellent long-term stability. The nanosheet-based TiO_2 microspheres with hollow core-shell structure, can be used for the efficient entrapment of other redox-active proteins and have wide potential applications in biosensors, biocatalysis, biomedical devices and bioelectronics.

1. Introduction

Enzyme immobilization has been shown to be a powerful tool to improve almost all enzyme properties, such as stability, activity, specificity, selectivity, and reduction of the effects of inhibitors [1–3]. Based on new developments in the field of enzyme immobilization, practical use of enzymes has been realized in various industrial processes and products, and is being expanded in new fields such as laboratory scale organic synthesis, biofuel cells, and medical and analytical applications [1,4,5]. In analytical applications, immobilized enzymes are used chiefly in biosensors [6,7], and the identity of the support and the immobilization technique can have a significant influence on the properties of the immobilized enzyme and performance of the biosensor [8,9].

Applications of the semiconductor material TiO_2 as catalyst supports [10–12] and in photocatalysis [13–15] have aroused increasing interest in recent years. Due to its good biocompatibility, relatively high conductivity, environmentally benign nature, and chemical and thermal stability, TiO_2 is a potential material for immobilization of enzymes [16–23]. Recently, TiO_2 in various forms, such as nanoparticles [16], nanotubes [17,18], nanosheets [19], three-dimensional macroporous matrices [20], and sol-gel matrices [21,22], have been extensively applied in developing biosensors. It has been shown that the morphology and structure of TiO_2 nanomaterials have an important effect on the property of the immobilized enzyme, which determines their efficacy in biosensors [9]. Although substantial effort has been devoted to the development of new nanostructured materials for use in biosensors, achieving controlled fabrication of new morphologies of TiO_2 nanostructures with high performance is still a challenge.

Hollow spheres with a complex core-shell structure have attracted significant attention recently for various applications including photocatalysis [24], battery materials [25,26], and sensing [27]. To the best of our knowledge, there has been no report of the application of hollow spheres with core-shell structure as a support for the enzyme immobilization. In this work, we have fabricated microspheres composed of TiO_2 nanosheets having a hollow core-shell structure using a simple hydrothermal method. Such a structure should have a number of advantages as a support for enzyme immobilization. As shown schematically in Fig. 1, by constructing the shell of the TiO_2 microspheres from a large number of nanosheets all pointing toward the center of the sphere, a large surface area is available for enzyme entrapment. The "trumpet"-shaped pores between the nanosheets are wider on the exterior of the shell and funnel the adsorbed enzyme toward the interior of the sphere where it can become immobilized on the

* Corresponding author. Tel.: +86 10 64435271; fax: +86 10 64425385.
E-mail address: yangws@mail.buct.edu.cn (W. Yang).

0142-9612/$ – see front matter © 2011 Elsevier Ltd. All rights reserved.
doi:10.1016/j.biomaterials.2011.05.055

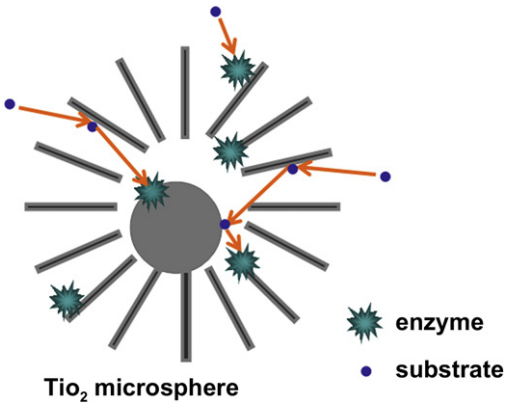

Fig. 1. Schematic illustration of the hollow core-shell structure of the nanosheet-based TiO_2 microspheres.

inner core of the microspheres. They also should increase the resistance of the enzyme to leaching during the reaction with the substrate. The substrate has easy access to the immobilized enzyme in the hollow interior of the core-shell structure and concentration of substrate and enzyme in this confined region will increase the chance of effective collisions between them. Hence, such a nanosheet-based hollow core-shell TiO_2 structure should be a promising support for enzyme immobilization and have potential applications in biosensors.

In this work, horseradish peroxidase (HRP) was selected as a model redox protein for construction of the H_2O_2 biosensor. The performance of a sensor composed of HRP immobilized in the nanosheet-based hollow core-shell TiO_2 microspheres was compared with that of sensors based on solid nanosheet-based TiO_2 microspheres, and the nanosheet-based hollow core-shell TiO_2 microspheres after destruction of the coreshell structure by high speed centrifugation, in order to highlight the advantages of the nanosheet-based hollow core-shell microsphere morphology as a support.

2. Experimental

2.1. Materials and apparatus

HRP (> 250 U mg^{-1}), titanium tetraisopropoxide (TTIP, Ti $[OCH(CH_3)_2]_4$, 97 wt.%) and Nafion (5 wt.% solution) were purchased from Sigma. Phosphate buffer solutions (PBS, 0.1 M) with different pH values were prepared by mixing standard stock solutions of Na_2HPO_4 and NaH_2PO_4. All other reagents were of analytical grade, and double distilled water was used throughout.

Scanning electron microscopy (SEM) images were obtained with a Zeiss Supra 55 scanning electron microscope at an accelerating voltage of 20 kV. Transmission electronic microscopy (TEM) images were obtained on a Hitachi H-800 instrument. The structures of the products were analyzed by powder X-ray diffraction (XRD), using a Shimadzu XRD-6000 diffractometer operated at 40 kV and 30 mA from 5° to 80° 2θ at the wavelength of Cu K_α radiation ($\lambda = 0.15406$ nm). UV–vis spectra were recorded using a Shimadzu UV-2501PC spectrophotometer. Specific surface area determination, and pore volume and pore size analysis were performed by Brunauer–Emmett–Teller (BET) and Barrett–Joyner–Halenda (BJH) methods, respectively, using a Quantachrome Autosorb-1C-VP analyzer. Prior to the measurements, samples were degassed at 200 °C for 2 h. Electrochemical measurements were carried out on a CHI 660B electrochemical workstation (Shanghai Chenhua Instrument Co.). A conventional three-electrode system was used, with the as-prepared immobilized HRP electrode as the working electrode, a platinum wire as the counter electrode, and a saturated Ag/AgCl electrode as the reference electrode.

2.2. Synthesis of TiO_2 microspheres

TiO_2 microspheres were synthesized by a controlled hydrothermal method using a titanate precursor. A solution of 0.5 M TTIP in ethylene glycol (20 mL) and 0.8 M lithium hydroxide solution (10 mL) were added to 0.25 M cetyltrimethylammonium bromide (CTAB) solution (20 mL). The resulting solution was mixed in an ultrasonic bath for 10 min and then transferred into a Teflon-lined stainless steel autoclave, which was sealed and maintained at 170 °C for a certain period of time. The precipitated powders were filtered, washed with ethanol and deionized water, dried at 80 °C and calcined at 300 °C in air for 2 h. The TiO_2 microspheres prepared with hydrothermal reaction times of 1 h, 3 h, 6 h, 12 h, 48 h, and 96 h are denoted as TiO_2–1, TiO_2–3, TiO_2–6, TiO_2–12, TiO_2–48 and TiO_2–96 respectively. The structure of TiO_2–48 was destroyed by centrifugation at 9000 rpm for 10 min and the resulting material is denoted D–TiO_2–48.

2.3. Encapsulation of HRP

10 mg of TiO_2–1, TiO_2–6 and TiO_2–48, were added to separate 3 mL aliquots of HRP solution (2 mg mL^{-1}). The resulting mixtures were continuously shaken at room temperature for 24 h to obtain HRP-entrapped TiO_2. The amount of entrapped HRP was measured by comparing the UV absorption at 403 nm of the supernatant solution before and after uptake of HRP by the TiO_2 samples.

2.4. Preparation of the enzyme electrode

Prior to use, a glassy carbon (GC) electrode with a diameter of 3 mm was successively polished on a polishing cloth with 1.0, 0.3, and 0.05 μm alumina powder and rinsed with deionized water. The electrode was then dried with a purified nitrogen stream. The enzyme electrode was prepared by a simple casting method. Firstly, a TiO_2 microsphere (such as TiO_2–1, TiO_2–6 or TiO_2–48) suspension was obtained by adding 2 mg of as-prepared TiO_2 microspheres into 1 mL of water with the aid of stirring. Then, a suspension, which finally contained 2.5 mg mL^{-1} of HRP, 1 mg mL^{-1} of TiO_2 and 1.25 wt.% of Nafion, was prepared by thoroughly mixing appropriate volumes of HRP solution (10 mg mL^{-1}, dissolved in pH 7.0 PBS), TiO_2 suspension (2 mg mL^{-1}) and Nafion solution (5 wt.%). Finally, 4 μL of the suspension was cast onto the surface of the freshly polished GC electrode to prepare the HRP/TiO_2/Nafion/GC electrode. The electrode was covered with a beaker so that water evaporated slowly in the air and a uniform film electrode was thus obtained. The dried HRP/TiO_2/Nafion/GC electrode was stored at 4 °C in a refrigerator when not in use. In control experiments, TiO_2–48/Nafion/GC and HRP/D–TiO_2–48/Nafion/GC electrodes were also prepared using similar procedures as described above.

3. Results and discussion

3.1. Characterization of TiO_2 microspheres

Fig. 2 shows SEM and TEM images depicting the TiO_2 microspheres formed with different hydrothermal reaction times, followed by calcination. The hydrothermal reaction time has a significant influence on the morphology of the as-synthesized TiO_2 microspheres. Uniform, smooth, and solid spherical particles (Fig. 2a) were obtained after reaction for 1 h. Small nanosheets

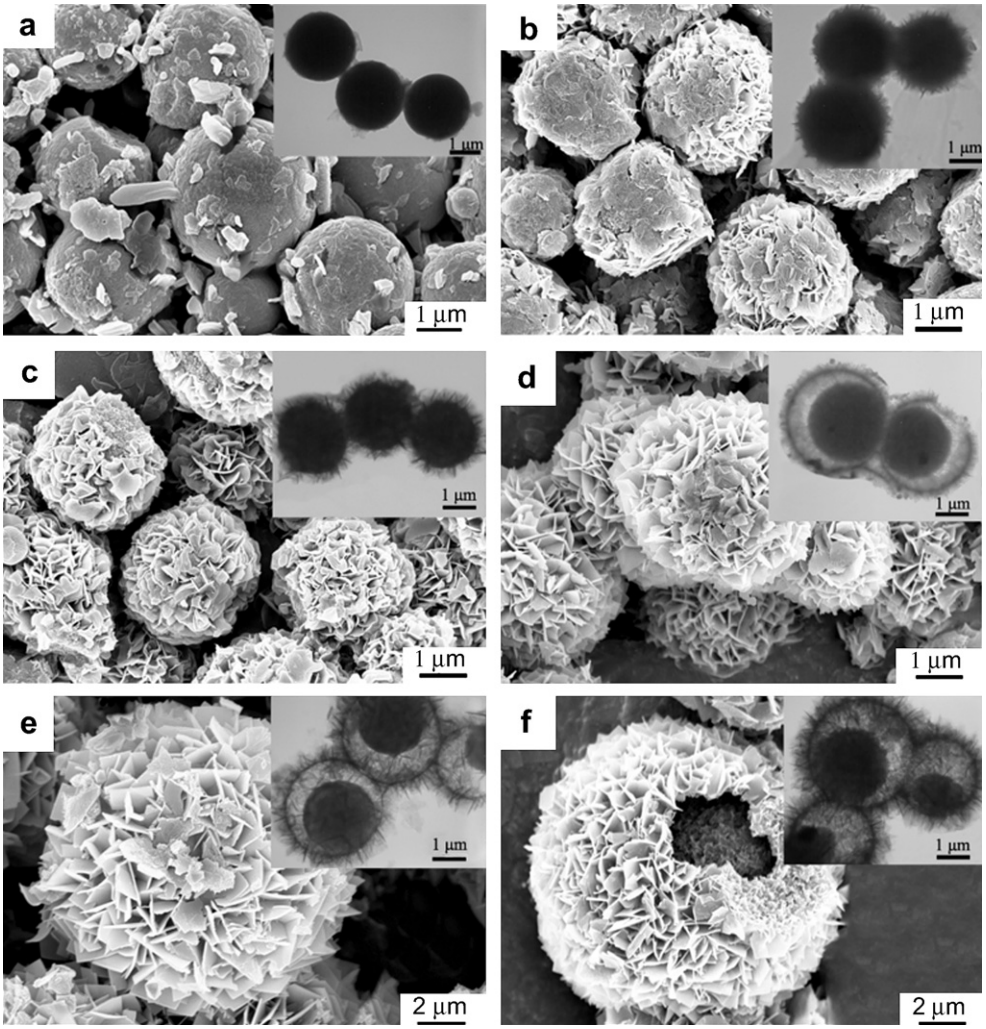

Fig. 2. SEM and TEM (insets) images of the calcined TiO_2 microspheres prepared with different hydrothermal reaction times: 1 h (a), 3 h (b), 6 h (c), 12 h (d), 48 h (e), and 96 h (f).

began to form on the surface after reaction for 3 h (Fig. 2b) and continued to grow with time, forming larger nanosheets (Fig. 2c–f). It was found that the nanosheet-based solid microspheres formed after reaction for 6 h (Fig. 2c). On increasing the hydrothermal reaction time to 12 h, a dramatic change in morphology occurred, with a transition from solid spherical particles to hollow core-shell structured spheres (Fig. 2d). The size of the cores continued to shrink with increasing hydrothermal reaction time (Fig. 2e–f). The images suggest that the products undergo an Ostwald ripening process [28,29] when the hydrothermal reaction time is prolonged. During this process, the inner crystallized nanoparticles of the core dissolve and redeposit and recrystallize on the nanosheets of the shell. Comparison of the images of the material synthesized with a hydrothermal reaction time of 48 h before (Figure S1) and after (Fig. 2e) calcination shows that the core-shell structure was not affected by the heat treatment. The hollow core-shell structure was however destroyed by centrifugation of the material at 9000 rpm for 10 min, as shown by the SEM image of the material D–TiO_2–48 in Figure S2.

The shell morphology and the core size of microspheres can therefore be easily tuned by controlling the hydrothermal reaction time. This suggests that if the reaction time is sufficiently long, the inner core will dissolve completely and a hollow sphere will result. However, prolonged reaction time resulted in disintegration of the structures, and in order to maintain the integrity of the microsphere structure, the longest hydrothermal reaction time employed in this work was 96 h.

Fig. 3 shows the X-ray diffraction (XRD) patterns of the products synthesized under hydrothermal conditions for 48 h before (Fig. 3a) and after (Fig. 3b) calcination at 300 °C for 2 h. The pattern of the sample before calcination indicates it is a mixture of titania and layered titanate species, since the peaks marked 101, 004, 200 are characteristic of the corresponding reflections of the anatase phase of titania [24,28] and the peak at 10.5° (d_{200} = 0.84 nm) is characteristic of a layered titanate structure [30]. Fig. 3b shows that the layered titanate is transformed to the anatase phase of TiO_2 after heat treatment at 300 °C, while maintaining the nanosheet-based hollow core-shell morphology. The strong and sharp diffraction peaks indicate the good crystallinity of the resulting TiO_2 spheres.

Since the morphologies of TiO_2 microspheres changed with increasing hydrothermal reaction time, three representative microspheres were chosen for further study, namely the smooth, solid TiO_2–1 microspheres, nanosheet-based solid TiO_2–6 microspheres and nanosheet-based hollow core-shell structured TiO_2–48 microspheres. As shown in Table 1, the most probable pore size of the microspheres increased as the reaction time was prolonged, whilst the surface area initially increased and then decreased with increasing reaction time. It is possible that with increasing reaction time, the crystallite nanoparticles dissolved giving the microspheres a more extended mesoporous structure,

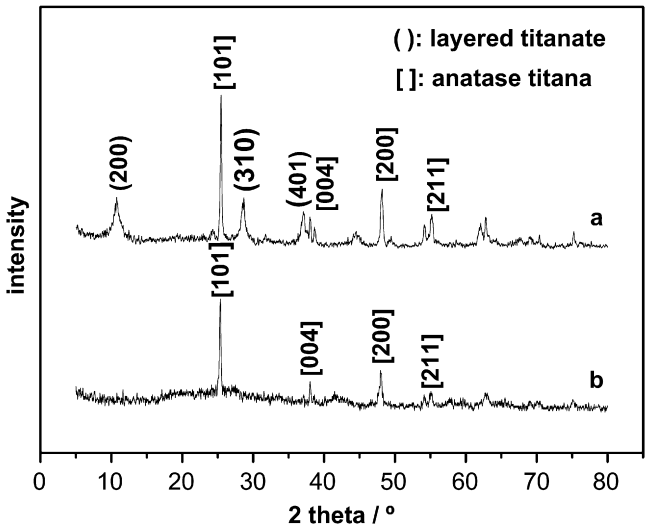

Fig. 3. XRD patterns of the products prepared by hydrothermal reaction for 48 h before (a) and after (b) calcination.

which resulted in the large increase in surface area. As the reaction time was prolonged however, the core of the spheres continued to dissolve creating the hollow core-shell structure. This results in a reduction in the amount of mesoporous structure in the core of the structure, leading to a reduction in surface area. The nanosheet-based hollow core-shell TiO_2–48 microsphere after destruction of the core-shell structure by high speed centrifugation was also studied. It was found that the specific surface area increased while the most probable pore size remained unchanged.

3.2. Encapsulation of HRP in the TiO_2 microspheres

HRP uptakes by the three microsphere samples TiO_2–1, TiO_2–6, TiO_2–48 and D–TiO_2–48 was studied, and the maximum loadings are given in Table 1. The uptake of HRP on TiO_2–6 microspheres was larger than on TiO_2–1, consistent with the larger surface area of the former. Interestingly, uptake of HRP on TiO_2–48 microspheres was even larger than for TiO_2–6 and D–TiO_2–48, despite the lower surface area of the former. Compared with solid spheres of a similar size (TiO_2–6), the hollow structure (TiO_2–48) enabled both the shell and core of the material to encapsulate HRP. Compared with TiO_2–48 microspheres after destruction of the core-shell structure (D–TiO_2–48), the hollow core-shell structure (TiO_2–48) increased the resistance of the adsorbed enzyme to leaching. Therefore the unique nanostructure and properties of the hollow core-shell TiO_2–48 microspheres make them particularly promising for applications in enzyme immobilization.

The Soret absorption bands of heme proteins provide information about the conformational integrity of the proteins. From Fig. 4, HRP entrapped in either a TiO_2–48 film (curve b) or a TiO_2–48/Nafion film (curve c) has a characteristic Soret absorption band at 403 nm, the same as that for the native state of a HRP film (curve a).

Table 1
Textural properties of TiO_2 microspheres prepared with different hydrothermal reaction times and TiO_2–48 after destruction.

Sample	Most probable pore size [nm]	BET surface area [m^2g^{-1}]	HRP loading [wt.%]
TiO_2–1	3	4.0	3.0
TiO_2–6	7	94.8	7.5
TiO_2–48	10	54.6	20.2
D–TiO_2–48	10	77. 5	19.8

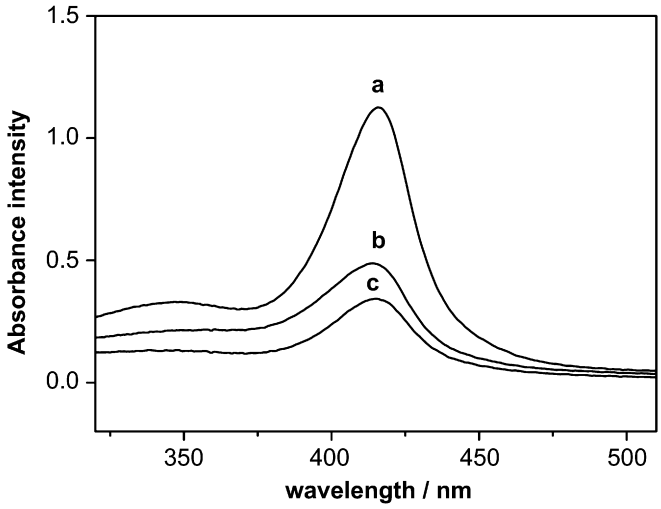

Fig. 4. UV–vis spectra of HRP (a), HRP/TiO_2 (b) and HRP/TiO_2/Nafion (c).

This suggests that the TiO_2 microspheres have good biocompatibility and do not lead to significant denaturation of the protein.

3.3. Direct electrochemistry of HRP at TiO_2/Nafion films

Fig. 5 depicts the typical cyclic voltammograms (CVs) of different modified electrodes in 0.1 M pH 7.5 PBS at a scan rate of 0.1 V s^{-1}. No redox peak is observed at the TiO_2–48/Nafion/GC electrode, which indicates TiO_2–48 is electroinactive in the potential window. HRP/Nafion/GC electrode shows slight redox peaks because the redox-active center of HRP is deeply seated in a cavity and therefore not easily accessible for conduction of electrons to the electrode surface. The HRP/TiO_2–48/Nafion/GC electrode exhibits a couple of stable redox peaks that are attributed to the redox of immobilized HRP. The formal potential ($E^{0'} = (E_{p,a} + E_{p,c})/2$) of HRP was −0.384 V vs. Ag/AgCl, characteristic of HRP-Fe(III)/HRP-Fe(II) redox couples previously reported in various films [31,32]. The potential difference (ΔE_p) between the anodic and cathodic peak potentials was about 52 mV. Such a small ΔE_p value is indicative of a fast and quasi-reversible electron transfer process, indicating TiO_2–48 can facilitate the electron transfer between the

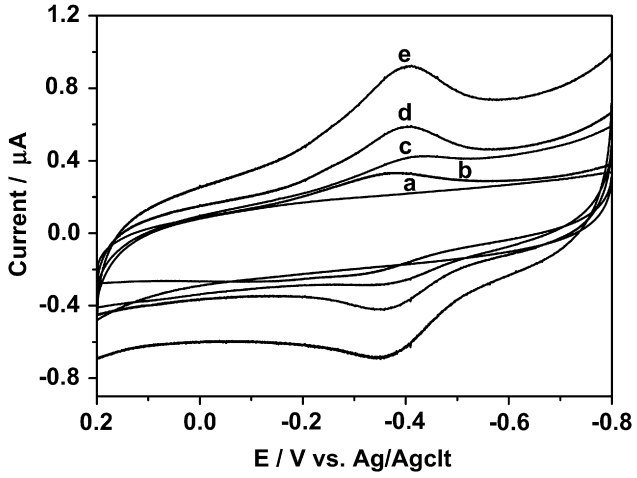

Fig. 5. Cyclic voltammograms of the TiO_2–48/Nafion/GC electrode (a), HRP/Nafion/GC electrode (b), HRP/TiO_2–1/Nafion/GC electrode (c), HRP/TiO_2–6/Nafion/GC electrode (d) and HRP/TiO_2–48/Nafion/GC electrode (e) in 0.1 M pH 7.5 PBS with a scan rate of 0.1 V s^{-1}.

electroactive center of HRP and electrode. For comparison, HRP/TiO_2–1/Nafion/GC and HRP/TiO_2–6/Nafion/GC electrodes have also been carried out (curve c and d in Fig. 5). The two electrodes also exhibit a couple of stable redox peaks with which the same formal potential of HRP/TiO_2–48/Nafion/GC electrode and the peak currents are smaller than that of HRP/TiO_2–48/Nafion/GC electrode. It results from the unique hollow core-shell structure of TiO_2–48, which has advantages on enzyme immobilization as described above and results in a large current response.

Fig. 6A shows the CVs of the HRP/TiO_2–48/Nafion/GC electrode with scan rates from 0.05 to 0.5 V s^{-1}. With increasing scan rates, the cathodic and anodic peak currents of HRP both increase, whilst the cathodic and anodic peak potentials show a small shift and the peak to peak separations become slightly enlarged. The cathodic and anodic peak currents increase linearly with scan rates from 0.05 to 0.5 V s^{-1}, as shown in Fig. 6B. This shows that the electron transfer between HRP and a GC electrode can be easily performed in the HRP/TiO_2–48/Nafion composite film and that a surface-controlled electrochemical process is involved. Using the Laviron method for a surface-controlled electrochemical system [33], the average electron transfer rate constant (k_s) of HRP immobilized on TiO_2–48/Nafion/GC was estimated to be about 5.4 s^{-1}, which is higher than the value reported for HRP immobilized on TiO_2 nanotube arrays (3.82 s^{-1}) [34], suggesting a faster electron transfer process. This means that the nanosheet-based hollow core-shell structure of TiO_2 microsphere facilitates the direct electron transfer of HRP.

The direct electrochemistry of HRP immobilized on the TiO_2–48/Nafion/GC electrode showed a strong dependence on solution pH. Fig. 7 shows the CVs of the HRP/TiO_2–48/Nafion/GC electrode in PBS with different pH values. CVs with stable and well-defined peaks were observed in the pH range 6.0–8.0, but increasing pH caused a negative shift of both cathodic and anodic peak potentials. This attributed to the involvement of proton transfer in the HRP-Fe(III)/HRP-Fe(II) redox couple. The $E^{0'}$ value of HRP varied linearly in the range of pH from 6.0 to 8.0, with a slope of −58.8 mV pH^{-1}. This value is very close to the theoretical value for the transfer of one proton and one electron in a reversible reduction (−58 mV pH^{-1} at 25 °C) [34].

3.4. Biosensor performance of the HRP/TiO_2/Nafion/GC electrode

When HRP is immobilized on an electrode surface with retention of its conformation, it normally exhibits electrocatalytic activity for oxygen, hydrogen peroxide, trichloroacetic acid, and nitrite. By using hydrogen peroxide as a probe, the electrocatalytic properties of the HRP/TiO_2/Nafion/GC electrode were studied. Fig. 8 shows the bioelectrocatalytic activity of the HRP/TiO_2–48/Nafion/GC electrode toward the reduction of H_2O_2 at a scan rate of 0.1 Vs^{-1}. A pair of reversible CV peaks appeared in the absence of H_2O_2 (curve a). Upon addition of H_2O_2 to the pH 7.5 PBS, the reduction peak current of immobilized HRP increased dramatically and the

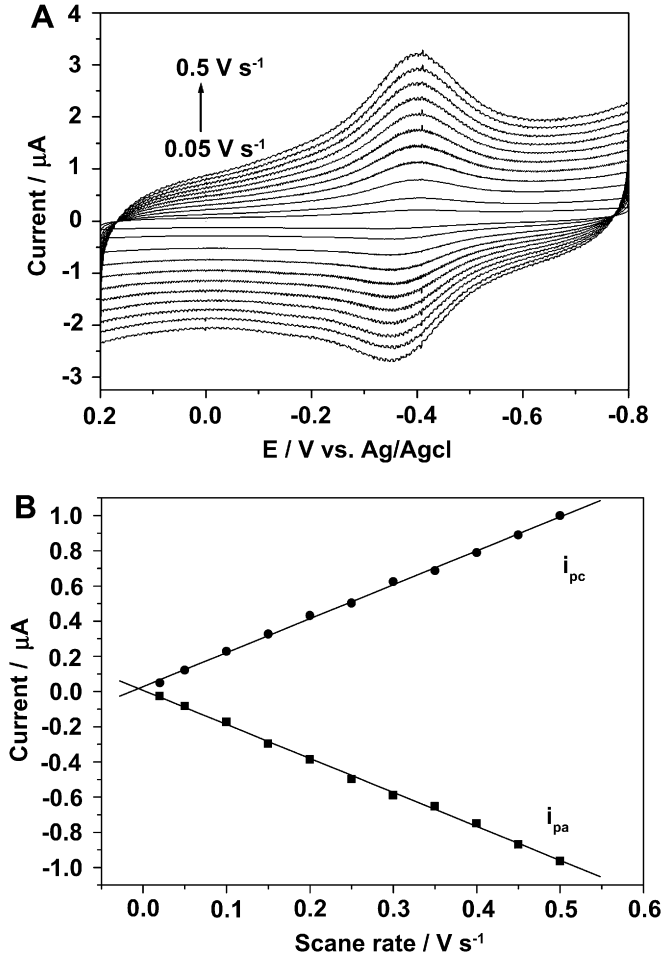

Fig. 6. (A) Cyclic voltammograms of the HRP/TiO_2–48/Nafion/GC electrode in 0.1 M pH 7.5 PBS with increasing scan rates from 0.05 to 0.5 V s^{-1}. (B) Plot of cathodic and anodic peak current vs. scan rate.

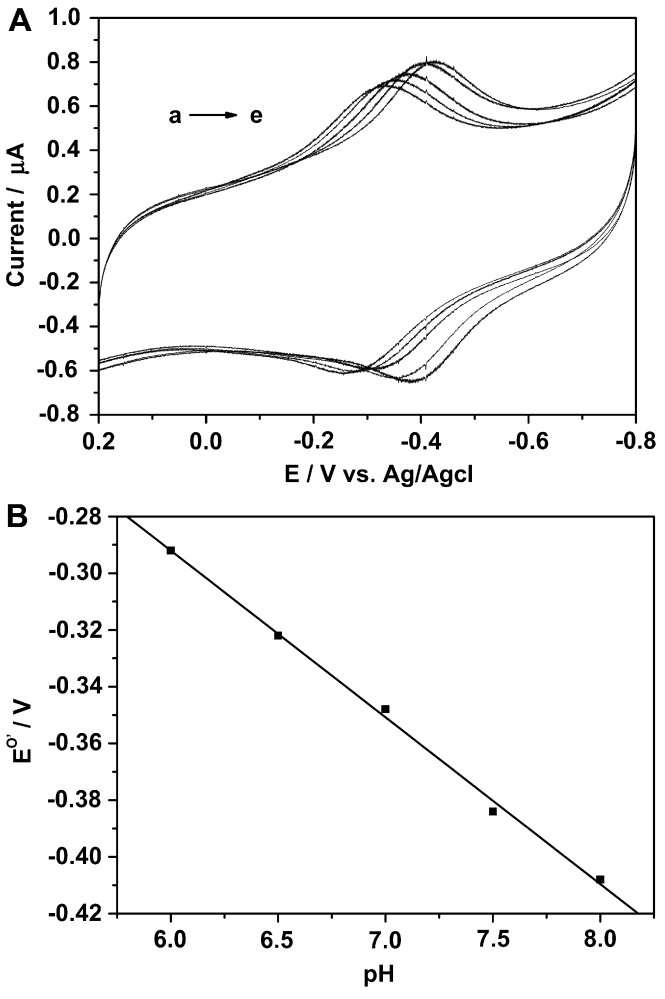

Fig. 7. (A) Cyclic voltammograms of the HRP/TiO_2–48/Nafion/GC electrode in 0.1 M PBS with different pH values: 6.0 (a), 6.5 (b), 7.0 (c), 7.5 (d), and 8.0 (e). (B) Plot of formal potential vs. pH value.

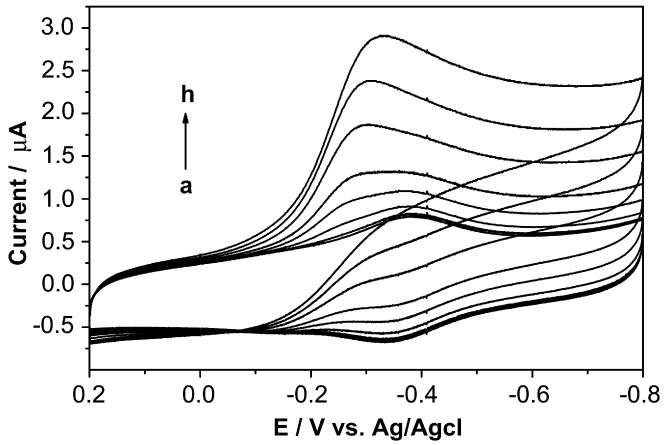

Fig. 8. Cyclic voltammograms of the HRP/TiO_2–48/Nafion/GC electrode in 0.1 M pH 7.5 PBS containing 0 (a), 3 (b), 10 (c), 25 (d), 50 (e), 80 (f), 130 (g), and 200 μM (h) H_2O_2 with a scan rate of 0.1 V s^{-1}.

oxidation peak current decreased. The reduction peak current increased with increasing H_2O_2 concentration (curves b–h), displaying the obvious electrocatalytic behavior of HRP for the reduction of H_2O_2 [35]. These results indicated that the immobilized HRP on TiO_2–48/Nafion film retains its electrocatalytic activity for the reduction of H_2O_2.

The biosensor performance of the HRP/TiO_2–48/Nafion/GC electrode was also studied by the amperometric current–time method. Fig. 9 illustrates a typical current–time curve of the HRP/TiO_2–48/Nafion/GC electrode at −0.35 V with successive addition of H_2O_2. When H_2O_2 was added to the stirred PBS, the reduction current increased rapidly and 95% of the steady-state current was obtained within 3 s (Fig. 9A). Moreover, a well-defined linear relationship between the current and the H_2O_2 concentration was observed. Under the optimized experimental conditions, the biosensor showed a very wide linear range in amperometric response to H_2O_2 ranging from 4.0×10^{-7} to 1.4×10^{-4} M, with a relative coefficient of 0.9999 (Fig. 9B). Table 2 shows a comparison of different H_2O_2 biosensors employing TiO_2 nanomaterials as an immobilization substrate. The morphology and structure of the nanomaterial has an important effect on the properties of the corresponding biosensor. Although high surface area materials such as nanoparticles [36], nanotubes [37], sol-gel [38], nanosheets [19] and three-dimensionally ordered macroporous materials can give a decrease in the detection limit of biosensor, their linear range is relatively narrow [20]. The hollow core-shell TiO_2–48 microsphere-based biosensor has both a low detection limit and wide linear range. Moreover, compared with TiO_2–1, TiO_2–6 and D–TiO_2–48 which do not have the hollow core-shell structure (Fig. 2a,c and Figure S2, respectively), the TiO_2–48 based biosensor has a wider linear range (Table 2 and Figure S3). There are several reasons why the TiO_2–48/Nafion composite has a lower detection limit whilst retaining a wider linear range. Firstly, both the outer shell and inner core of the TiO_2–48 microspheres can provide a protective microenvironment for the enzyme, allowing it to retain its stability and activity. More importantly, the pores formed by the accumulation of nanosheets are "trumpet" shaped. The open framework of the pores allows the substrate to easily enter the sphere and in the confined space of the core-shell hollow structure, there is an increased chance of effective collisions between substrate and enzyme leading to improved performance of the enzyme electrode.

The long-term stability of fabricated biosensor was investigated by examining its current response after storage in a refrigerator at 4 °C. The biosensor exhibited no obvious decrease in current response in the first week and maintained about 95% of its initial

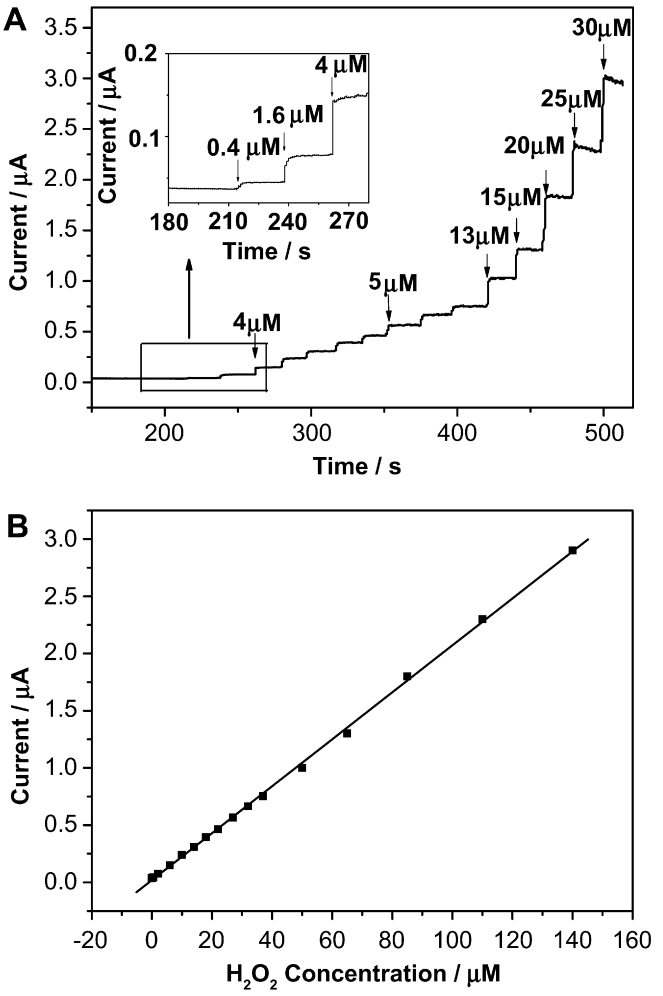

Fig. 9. (A) Typical current-time response of the HRP/TiO_2–48/Nafion/GC electrode at −0.35 V to successive addition of H_2O_2 in a stirred 0.1 M pH 7.5 PBS. (B) Plot of steady-state current vs. H_2O_2 concentration.

value after three weeks. The relative standard deviation (R.S.D.) of the biosensor response to 10 μM H_2O_2 for 5 successive measurements was 2.1%. Five electrodes were prepared utilizing the same method to check the reproducibility of the biosensor. When detecting the same concentration of 10 μM H_2O_2, the results

Table 2
Comparison of the performances of various H_2O_2 biosensors employing different TiO_2 nanomaterials as an immobilization substrate.

Modifed electrode	Linear range (μM)	Detection limit (μM)	Response time (s)	References
HRP/TiO_2–48/Nafion/GCE	0.4–140	0.05	3	This work
HRP/TiO_2–1/Nafion/GCE	0.4–28	0.1	3	This work
HRP/TiO_2–6/Nafion/GCE	0.4–60	0.1	3	This work
HRP/D–TiO_2–48/Nafion/GCE	0.4–15	0.1	3	This work
Nafion/HRP–GNSs–TiO_2 colloids/GCE	41–630	5.9	3	35
HRP–TiO_2 nanoparticle/PGE	7.5–123	2.5		36
TiO_2 sol–gel/HRP/GCE	80–560	1.5	5	38
HRP/3DOM TiO_2/OTE	0.5–6	0.01		20
HRP/Au/TiO_2 nanotube arrays/Ti	5–400	2.0	5	37
HRP/TiO_2 nanosheet/GCE	2.1–185	0.7		19

GNSs, gold nano-seeds (2–5 nm); PGE, pyrolytic graphite electrode; 3DOM, three-dimensionally ordered macroporous; OTE, optically transparent electrode.

showed a R.S.D. of 2.9%, indicating an acceptable electrode-to-electrode reproducibility.

4. Conclusions

Nanosheet-based TiO_2 microspheres with a tailorable hollow core-shell structure have been successfully fabricated through a facile hydrothermal method followed by calcination. The unique TiO_2 microspheres have been verified to be a good immobilization matrix for HRP and the prepared mediator-free biosensor possesses good performance, especially displays both a lower detection limit and a wider linear range than those other morphological TiO_2 nanomaterials. The improved performance of the biosensor can be contributed to the unique structure of TiO_2 microspheres, whose outer shell and inner core can immobilize enzymes. More importantly, in the confined space of the hollow core-shell structure there is an increased chance of effective collisions between substrate and enzyme. The nanosheet-based TiO_2 microspheres with hollow core-shell structure have been proved to be a promising matrix for the fabrication of electrochemical biosensors, and may find wide potential applications in biomedical detection and environmental analysis.

Acknowledgments

This work was supported by National Natural Science Foundation of China (Grant No. 20971011), the National Basic Research Program of China (Grant No. 2011CBA00508), the Beijing Natural Science Foundation (Grant No. 8102028), the Program for New Century Excellent Talents in Universities (Grant No. NCET-08-0713), and the Fundamental Research Funds for the Central Universities (Grant No. ZD1004).

Appendix. Supplementary material

Supplementary data associated with this article can be found, in the online version, at doi:10.1016/j.biomaterials.2011.05.055.

References

[1] Barbara K. Application of chitin- and chitosan-based materials for enzyme immobilizations: a review. Enzym Microb Tech 2004;35:126–39.
[2] Henrik K, Maria K. The use of magnetite nanoparticles for implant-assisted magnetic drug targeting in thrombolytic therapy. Biomaterials 2010;31:9499–510.
[3] Pedro T. Sub-100 nm TiO_2 mesocrystalline assemblies with mesopores: preparation, characterization, enzyme immobilization and photocatalytic properties. Chem Commun 2011;47:256–8.
[4] Ball P. Biocatalysis. Nat 2001;409:225.
[5] van de Velde F, Lourenço ND, Pinheiro HM, Bakker M. Carrageenan: a food-grade and biocompatible support for immobilisation techniques. Adv Synth Catal 2002;344:815–35.
[6] Wilson GS, Hu YB. Enzyme-based biosensors for in vivo measurements. Chem Rev 2000;100:2693–704.
[7] Yang Z, Zong XL, Ye ZZ, Zhao BH, Wang QL, Wang P. The application of complex multiple forklike ZnO nanostructures to rapid and ultrahigh sensitive hydrogen peroxide biosensors. Biomaterials 2010;31:7534–41.
[8] Cesar M, Jose MP, Gloria F-L, Jose MG, Roberto F-L. Improvement of enzyme activity, stability and selectivity via immobilization techniques. Enzym Microb Tech 2007;40:1451–63.
[9] Kim JB, Grate JW, Wang P. Nanostructures for enzyme stabilization. Chem Eng Sci 2006;61:1017–26.
[10] Wu ZJ, Zhao ZF, Zhang MH. Synthesis by replacement reaction and application of TiO_2-supported Au-Ni bimetallic catalyst. ChemCatChem 2010;2:1606–14.
[11] Do TB, Cai M, Ruthkosky MS, Moylan TE. Niobium-doped titanium oxide for fuel cell application. Electrochim Acta 2010;55:8013–7.
[12] Karakotia AS, King JES, Vincent A, Seal S. Synthesis dependent core level binding energy shift in the oxidation state of platinum coated on ceria–titania and its effect on catalytic decomposition of methanol. Appl Catal A–Gen 2010;388:262–71.
[13] Carp O, Huisman CL, Reller A. Photoinduced reactivity of titanium dioxide. Prog Solid State Ch 2004;32:33–177.
[14] Lachheb H, Puzenat E, Houas A, Ksibi M, Elaloui E, Guillard C, et al. Photocatalytic degradation of various types of dyes (Alizarin S, Crocein Orange G, Methyl Red, Congo Red, Methylene Blue) in water by UV-irradiated titania. Appl Catal B Environ 2002;39:75–90.
[15] Chen XB, Lou YB, Samia ACS, Burda C, Gole JL. Formation of oxynitride as the photocatalytic enhancing site in nitrogen-doped titania nanocatalysts: comparison to a commercial nanopowder. Adv Funct Mater 2005;15:41–9.
[16] Shi YT, Yuan R, Chai YQ, Tang MY, He XL. Amplification of antigen–antibody interactions via back-filling of HRP on the layer-by-layer self-assembling of thionine and gold nanoparticles films on titania nanoparticles/gold nanoparticles-coated Au electrode. J Electroanal Chem 2007;604:9–16.
[17] Liu S, Chen A. Coadsorption of horseradish peroxidase with thionine on TiO_2 nanotubes for biosensing. Langmuir 2005;21:8409–13.
[18] Xie YB, Zhou LM, Huang HT. Bioelectrocatalytic application of titania nanotube array for molecule detection. Biosens Bioelectron 2007;22:2812–8.
[19] Zhang L, Zhang Q, Lu XB, Li JH. Direct electrochemistry and electrocatalysis based on film of horseradish peroxidase intercalated into layered titanate nano-sheets. Biosens Bioelectron 2007;23:102–6.
[20] Zhu YH, Cao HM, Tang LH, Yang XL, Li CZ. Immobilization of horseradish peroxidase in three-dimensional macroporous TiO_2 matrices for biosensor applications. Electrochim Acta 2009;54:2823–7.
[21] Doong RA, Shih HM. Glutamate optical biosensor based on the immobilization of glutamate dehydrogenase in titanium dioxide sol–gel matrix. Biosens Bioelectron 2006;22:185–91.
[22] Yu JH, Liu SQ, Ju HX. Glucose sensor for flow injection analysis of serum glucose based on immobilization of glucose oxidase in titania sol–gel membrane. Biosens Bioelectron 2003;19:401–9.
[23] Luckarift HR, Dickerson MB, Sandhage KH, Spain JC. Rapid, room-temperature synthesis of antibacterial bionanocomposites of lysozyme with amorphous silica or titania. Small 2006;2:640–3.
[24] Li HX, Bian ZF, Zhu J, Zhang DQ, Li GS, Huo YN, et al. Mesoporous titania spheres with tunable chamber structure and enhanced photocatalytic activity. J Am Chem Soc 2007;129:8406–7.
[25] Deng D, Lee JY. Hollow core-shell mesospheres of crystalline SnO_2 nanoparticle aggregates for high capacity Li^+ ion storage. Chem Mater 2008;20:1841–6.
[26] Wang X, Wu XL, Guo YG, Zhong YT, Cao XQ, Ma Y, et al. Synthesis and lithium storage properties of Co_3O_4 nanosheet-assembled multishelled hollow Spheres. Adv Funct Mater 2010;20:1680–6.
[27] Sattarahmady N, Heli H, Moosavi-Movahedi AA. An electrochemical acetylcholin biosensor based on nanoshells of hollow nickel microspheres-carbon microparticles-Nafion nanocomposite. Biosens Bioelectron 2010;25:2329–35.
[28] Cui YM, Liu L, Li B, Zhou XF, Xu NP. Fabrication of tunable core-shell structured TiO_2 mesoporous microspheres using linear polymer polyethylene glycol as templates. J Phys Chem C 2010;114:2434–9.
[29] Yang HG, Zeng HC. Preparation of hollow anatase TiO_2 nanospheres via Ostwald ripening. J Phys Chem B 2004;108:3492–5.
[30] Tang YF, Yang L, Fang SH, Qiu Z. $Li_4Ti_5O_{12}$ hollow microspheres assembled by nanosheets as an anode material for high-rate lithium ion batteries. Electrochim Acta 2009;54:6244–9.
[31] Xu Q, Mao C, Liu NN, Zhu JJ, Sheng J. Direct electrochemistry of horseradish peroxidase based on biocompatible carboxymethyl chitosan-gold nanoparticle nanocomposite. Biosens Bioelectron 2006;22:768–73.
[32] Xiao XL, Luan QF, Yao X, Zhou KB. Single-crystal CeO_2 nanocubes used for the direct electron transfer and electrocatalysis of horseradish peroxidase. Biosens Bioelectron 2009;24:2447–51.
[33] Laviron E. General expression of the linear potential sweep voltammogram in the case of diffusionless electrochemical systems. J Electroanal Chem 1979;101:19–28.
[34] Wu FH, Xu JJ, Tian Y, Hu ZC, Wang LW, Xian YZ, et al. Direct electrochemistry of horseradish peroxidase on TiO_2 nanotube arrays via seeded-growth synthesis. Biosens Bioelectron 2008;24:198–203.
[35] Wang Y, Ma XL, Wen Y, Xing YY, Zhang ZR, Yang HF. Direct electrochemistry and bioelectrocatalysis of horseradish perxidase based on gold nano-seeds dotted TiO_2 nanocomposite. Biosens Bioelectron 2010;25:2442–6.
[36] Zhang Y, He PL, Hu NF. Horseradish peroxidase immobilized in TiO_2 nanoparticle films on pyrolytic graphite electrodes: direct electrochemistry and bioelectrocatalysis. Electrochim Acta 2004;49:1981–8.
[37] Kafi AKM, Wu GS, Chen AC. A novel hydrogen peroxide biosensor based on the immobilization of horseradish peroxidase onto Au-modified titanium dioxide nanotube arrays. Biosens Bioelectron 2008;24:566–71.
[38] Yu JH, Ju HX. Preparation of porous titania sol-gel matrix for immobilization of horseradish peroxidase by a vapor deposition method. Anal Chem 2002;74:3579–83.